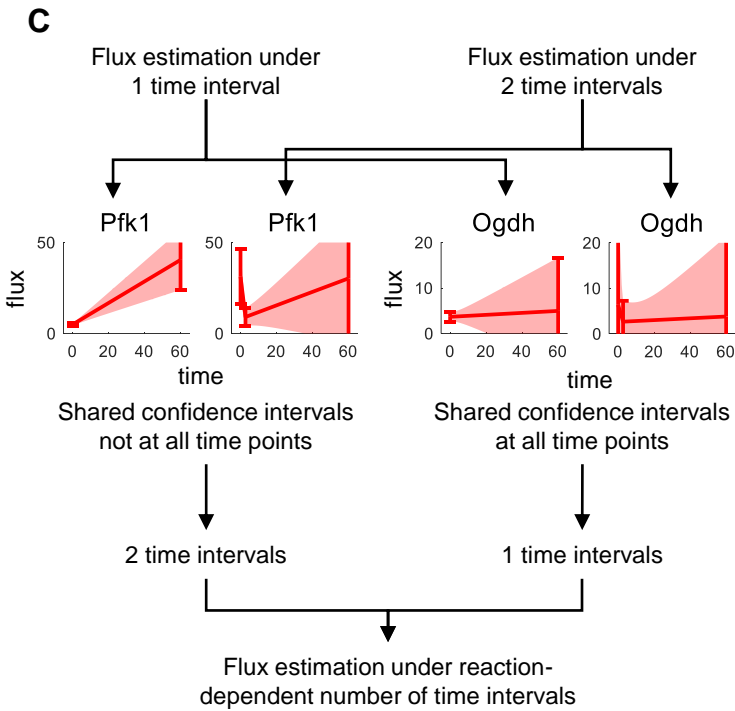
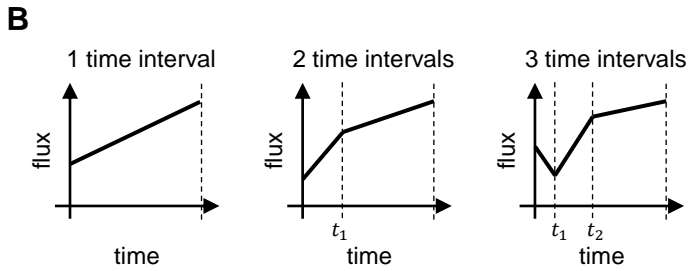
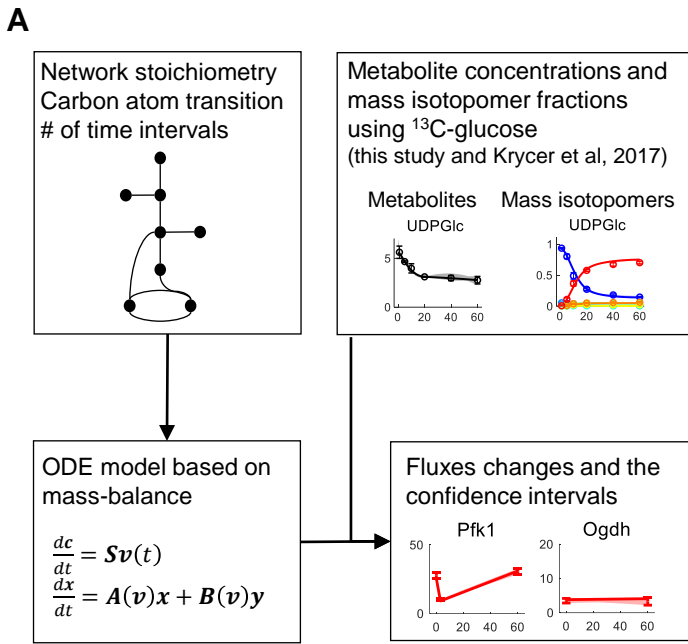


iScience, Volume 23

Supplemental Information

Kinetic Trans-omic Analysis Reveals Key Regulatory Mechanisms for Insulin-Regulated Glucose Metabolism in Adipocytes

Satoshi Ohno, Lake-Ee Quek, James R. Krycer, Katsuyuki Yugi, Akiyoshi Hirayama, Satsuki Ikeda, Futaba Shoji, Kumi Suzuki, Tomoyoshi Soga, David E. James, and Shinya Kuroda



D

# of time intervals	z-score to determine # of time intervals	# of parameters	RSS	AIC
1	-	212	4991	2112
2	-	335	2199	1415
3	-	458	1906	1497
	4.00	231	3929	1875
	3.00	249	3325	1719
	2.00	266	2857	1579
	1.50	273	2693	1525
reaction dependent	1.00	281	2678	1534
	0.75	294	2546	1502
	0.60	315	2242	1397
	0.50	329	2212	1410
	0.40	346	2128	1400
	0.30	377	2081	1436

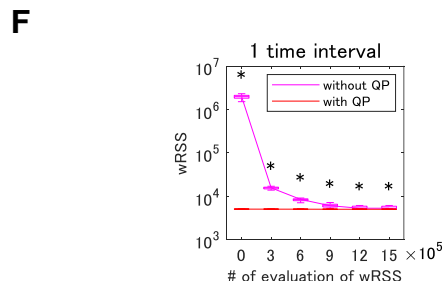
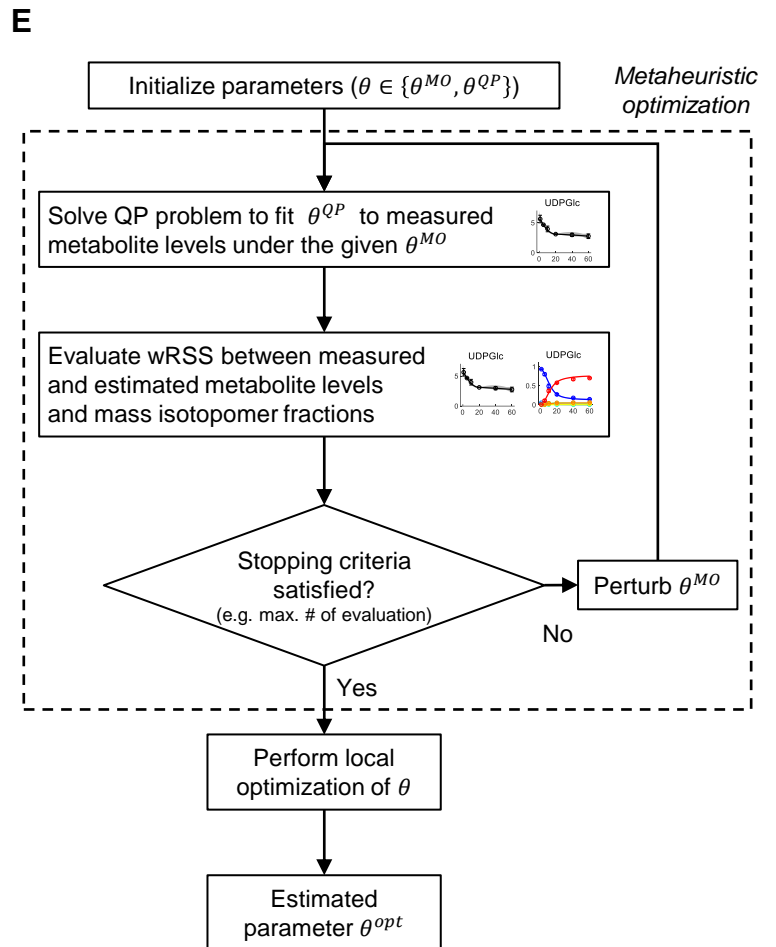


Figure S1. Procedures of estimation of flux changes under non-steady-state conditions. Related to Figures 2 and 3.

(A) Overview of estimation of flux changes under non-steady-state conditions.

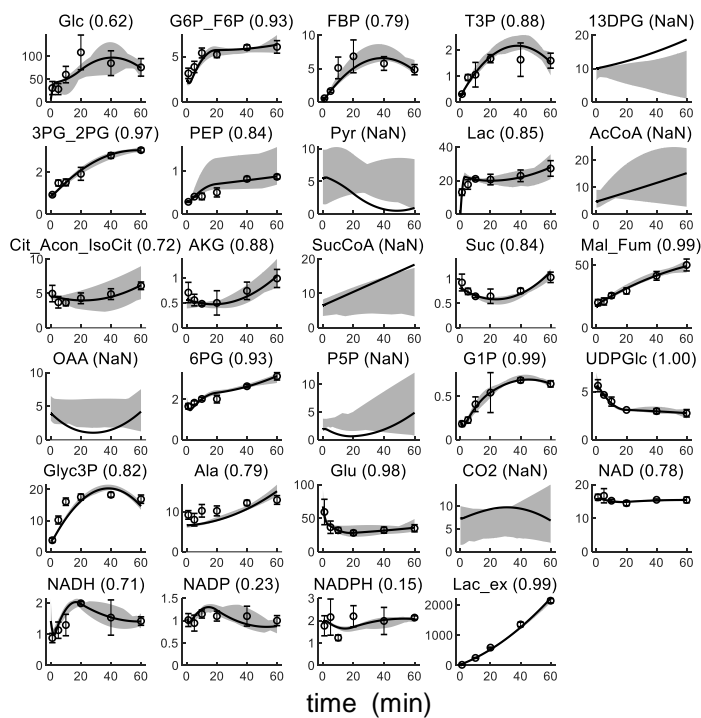
(B) Flux described as a piecewise linear function in the time domain with switch times (times when the slope of flux changes). The switch times are represented as t_1 under 2 time intervals, and as t_1 and t_2 under 3 time intervals.

(C) Determination of reaction-dependent number of time intervals (see Transparent Methods).

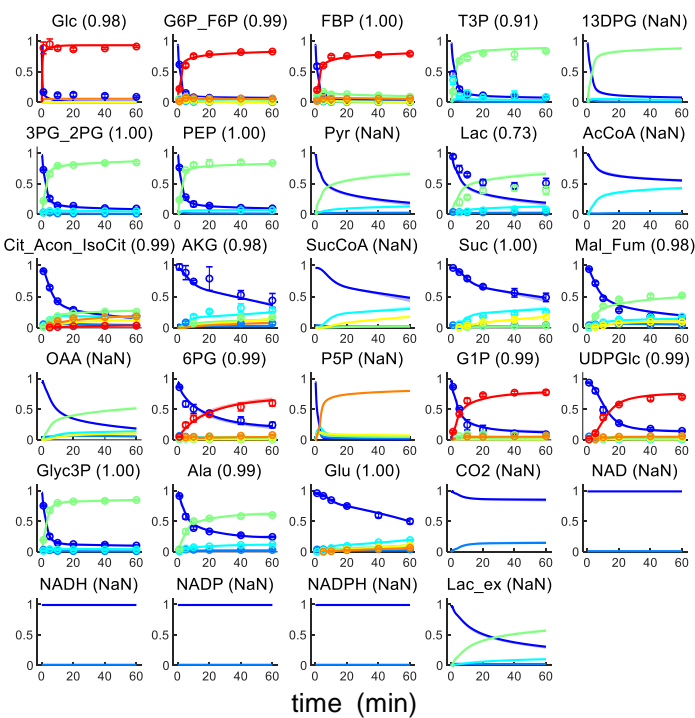
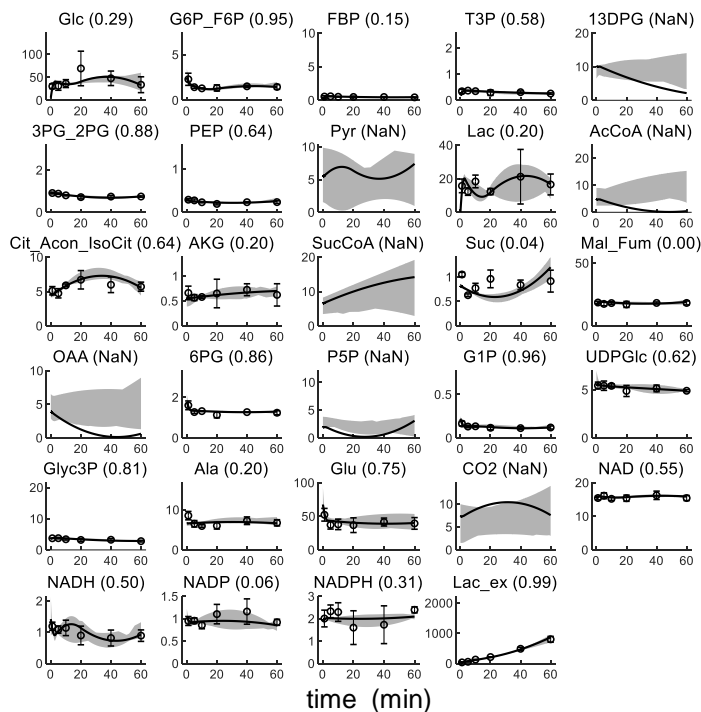
(D) AIC of the models with the same number of time intervals among all reactions and the model with reaction-dependent number of time intervals. AIC is defined as $N \log(\text{wRSS}/N) + 2p$, where N is the number of residuals and p is the number of parameters.

(E) Optimization procedure of parameters using quadratic programming (QP) (see Transparent Methods).

(F) Convergence profiles of metaheuristic optimization with or without use of QP under one time interval. The same number of time intervals was set among all reactions. The lines connect the median values among 30 independent optimizations. The box encompasses the 25th to 75th percentiles, and the whiskers indicate the maximum and minimum values. The medians of the wRSS were compared between optimizations with and without use of QP using Wilcoxon rank-sum test with the Bonferroni multiple testing correction. P values < 0.01 were considered statistically significant and are indicated with an asterisk (*). Metaheuristic optimization without use of QP under two and three time intervals was not able to be performed under our optimization condition because initial parameters in the optimization were not updated even after one week.

A**Ins** Metabolite concentrations (nmol/mg-protein)

Mass isotopomer fractions

**Ctrl** Metabolite concentrations (nmol/mg-protein)

Mass isotopomer fractions

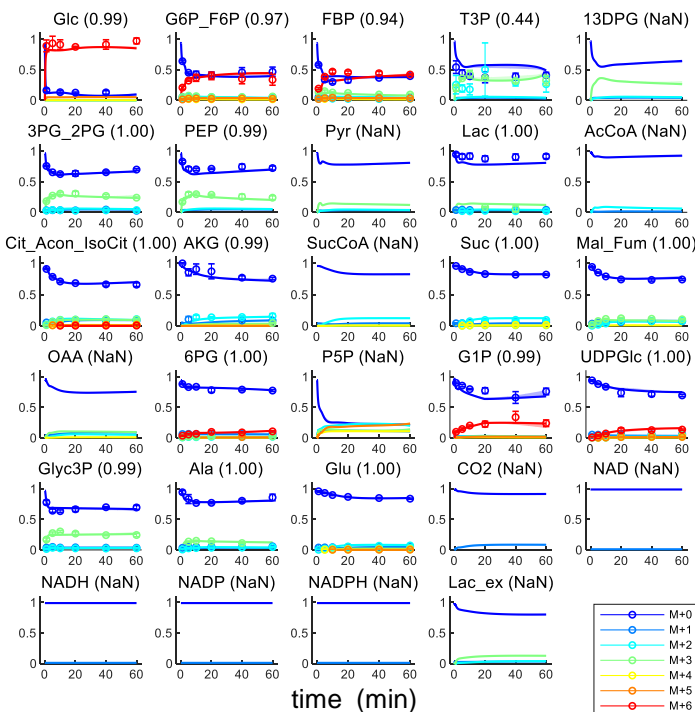
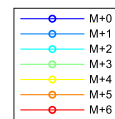
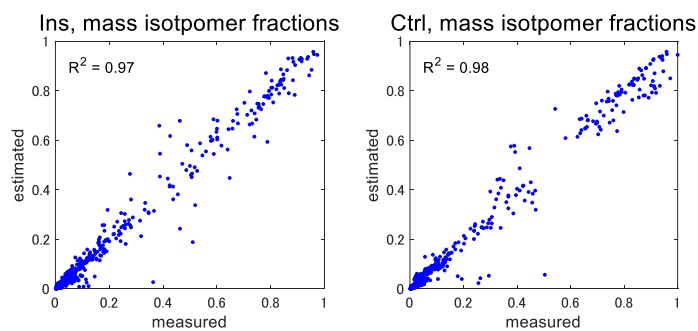
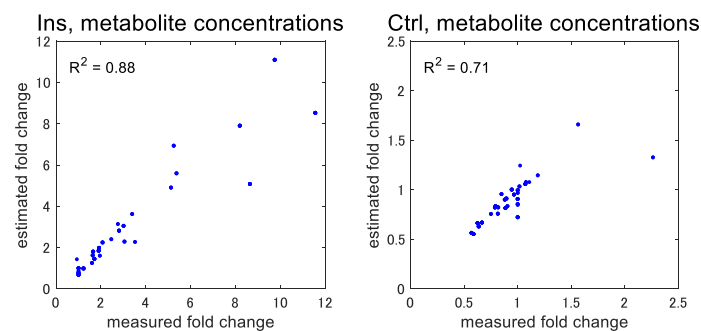
**B**

Figure S2. All measured and estimated metabolite concentrations and mass isotopomer fractions. Related to Figure 2.

(A) All measured and estimated metabolite concentrations and mass isotopomer fractions. The circles and the error bars indicate the mean and the standard deviations of the measurements from 3 separate experiments (Krycer et al., 2017). The lines and the shaded areas indicate optimal estimates with the 90% confidence intervals. M+*i* indicates mass isotopomer with *i* carbons labelled with ¹³C. The numbers next to the metabolite names indicates R² values between measured and estimated concentrations or mass isotopomer fractions. Note that media were exchanged at 0 min in both the conditions. The optimal estimates can be outside the confidence intervals due to sampling from a truncated multivariate normal distribution and the curse of dimensionality (Verleysen and François, 2005). Abbreviations of metabolites are defined in Table S1, and the data of estimated concentrations are shown in Table S2.

(B) Scatter plots of all measured and estimated metabolite concentrations and mass isotopomer fractions. Measured and estimated metabolite concentrations are shown as fold changes to measured concentrations at 1 min.

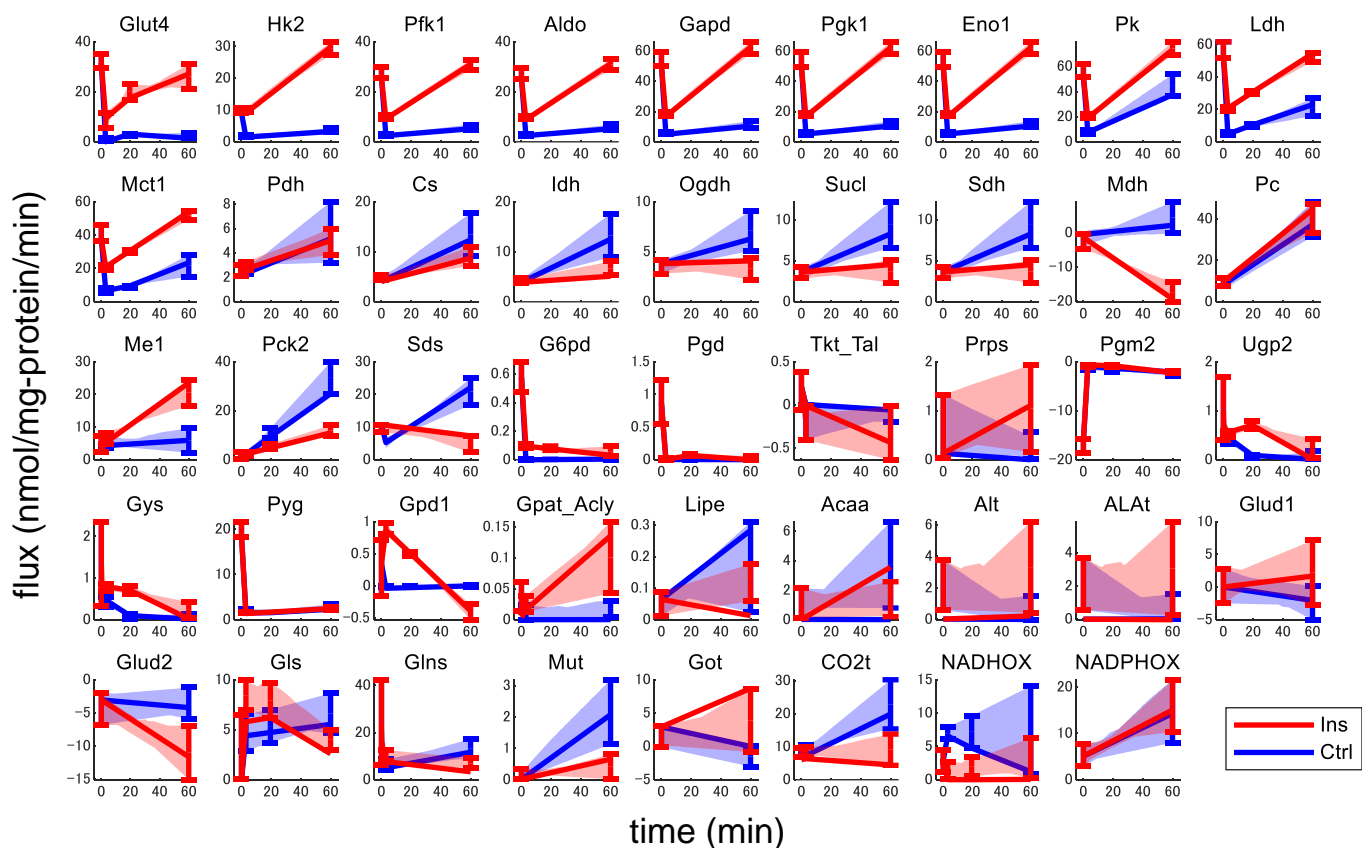
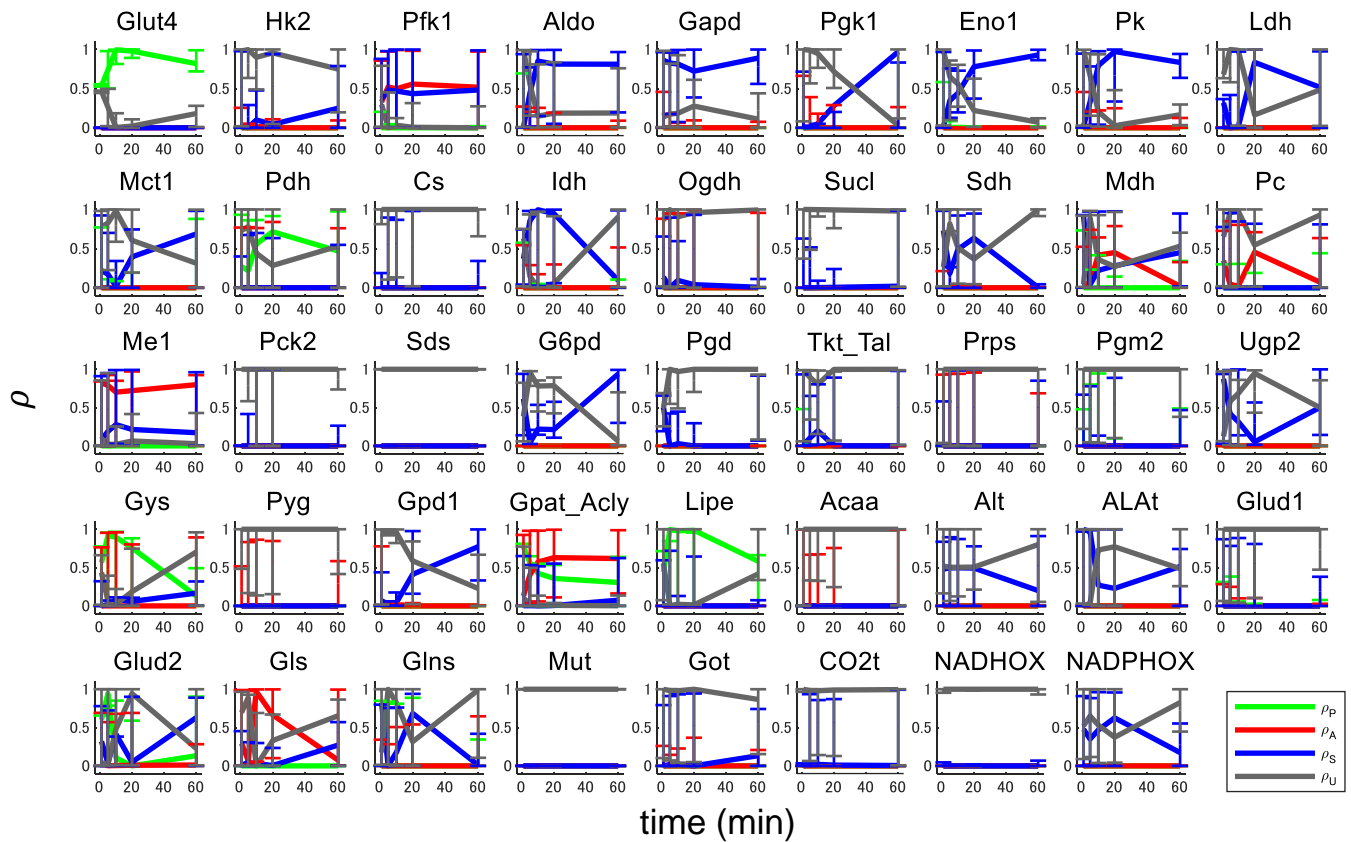


Figure S3. All estimated flux changes. Related to Figure 3.

The lines and the shaded areas indicate optimal estimates (Table S2) with the 90% confidence intervals. Error bars indicate the 90% confidence intervals at switch times (times when the slope of flux changes), as well as 0 and 60 min. Number of time intervals (and switch times) were set among reactions (see Transparent Methods). The confidence intervals were calculated from 200 sets of sampled parameters under constraints based on the covariance matrix of the estimated parameters (see Transparent Methods). Note that the optimal estimates can be outside the confidence intervals due to sampling from a truncated multivariate normal distribution and the curse of dimensionality (Verleysen and François, 2005). Abbreviations of reactions are defined in Table S1, and the data of estimated fluxes are shown in Table S2.

A



B

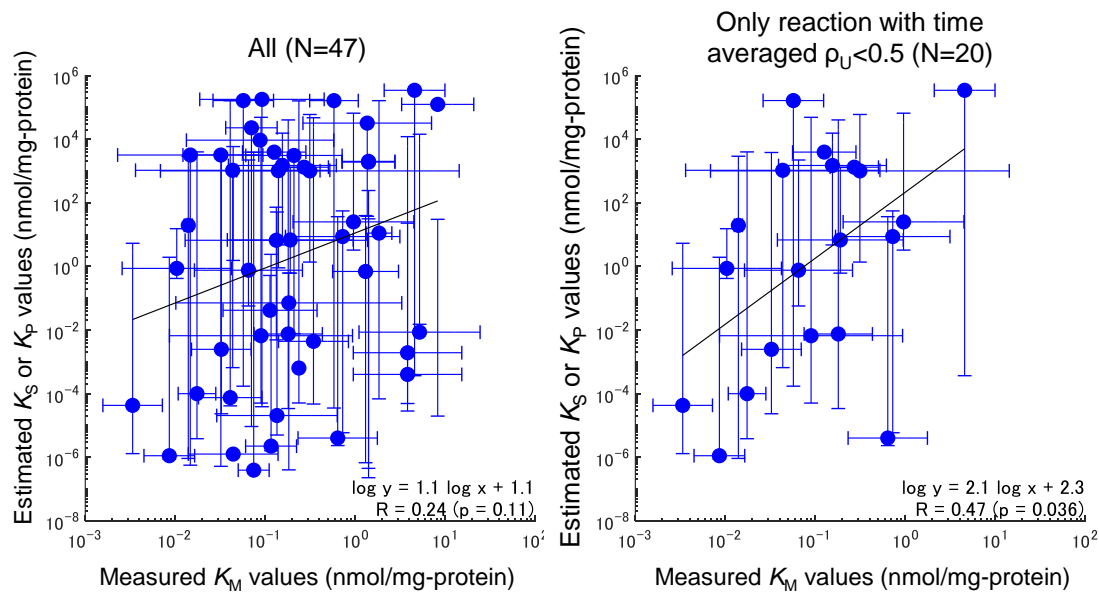
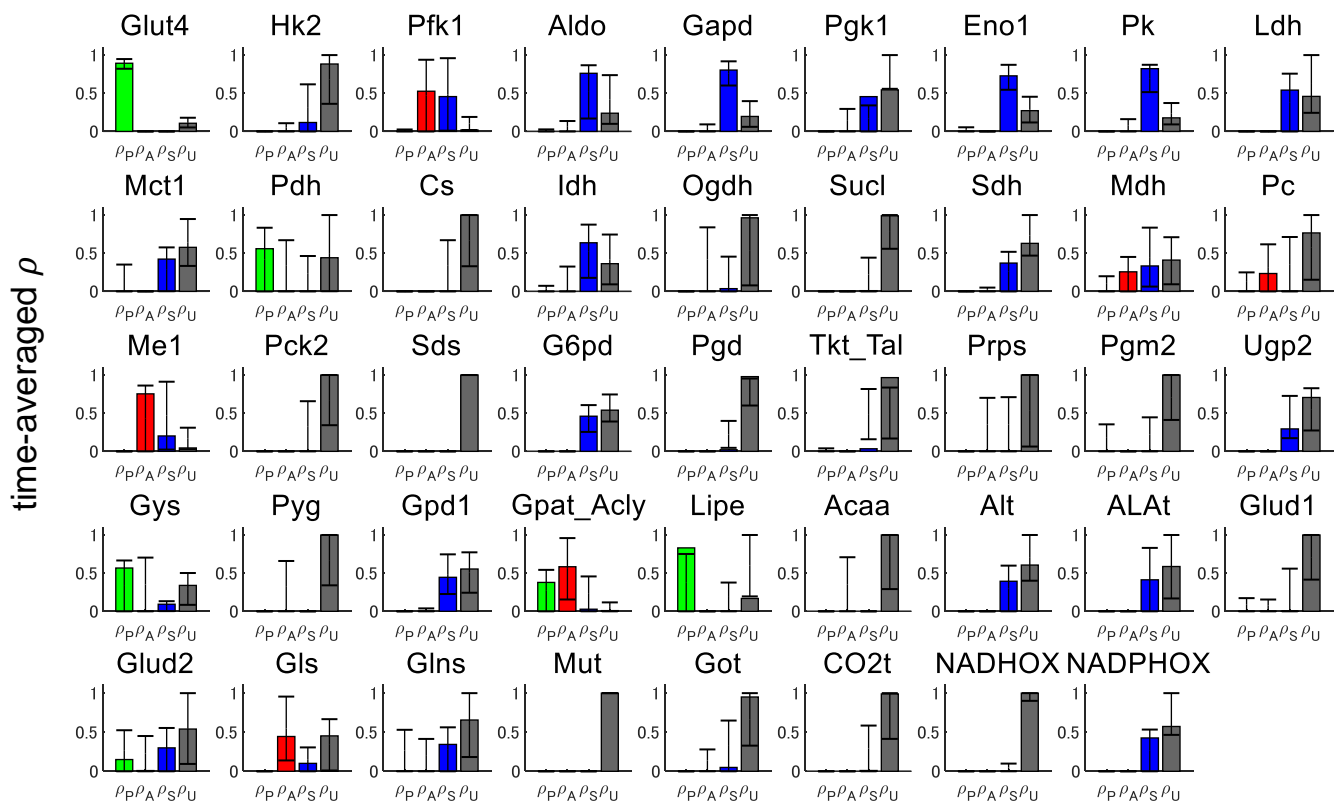


Figure S4. Time courses of regulation coefficients and comparison of Michaelis-Menten constants estimated in this study with those experimentally measured. Related to Figure 5.

(A) Time courses of regulation coefficients of enzyme phosphorylation (ρ_P), allosteric effectors (ρ_A), substrates and products (ρ_S), and unaccounted regulators (ρ_U). The regulation coefficients were calculated at 1, 5, 10, 20, and 60 min. The lines indicate regulation coefficients calculated from optimal estimates of parameters in our metabolic flux analysis. Error bars indicate the 90% confidence intervals. The confidence intervals were calculated from 200 sets of sampled parameters (see Transparent Methods). Abbreviations of reactions are defined in Table S1.

(B) Comparison of Michaelis-Menten constants estimated in this study with those reported in the BRENDA database for all reaction (left) and for only reaction with the time averaged ρ_U smaller than 0.5 (right). The dots represent the geometric mean of the measured K_M values versus estimated K_S or K_P values using optimal flux estimates in the metabolic flux analysis. The error bars of measured values represent the geometric standard deviations and the error bars of estimated values represent 90% confidence intervals, calculated from 200 sets of sampled parameters. N represents the number of dots. The regression lines of the dots, Pearson's correlation coefficients (R), and the p-values are shown.

A



B

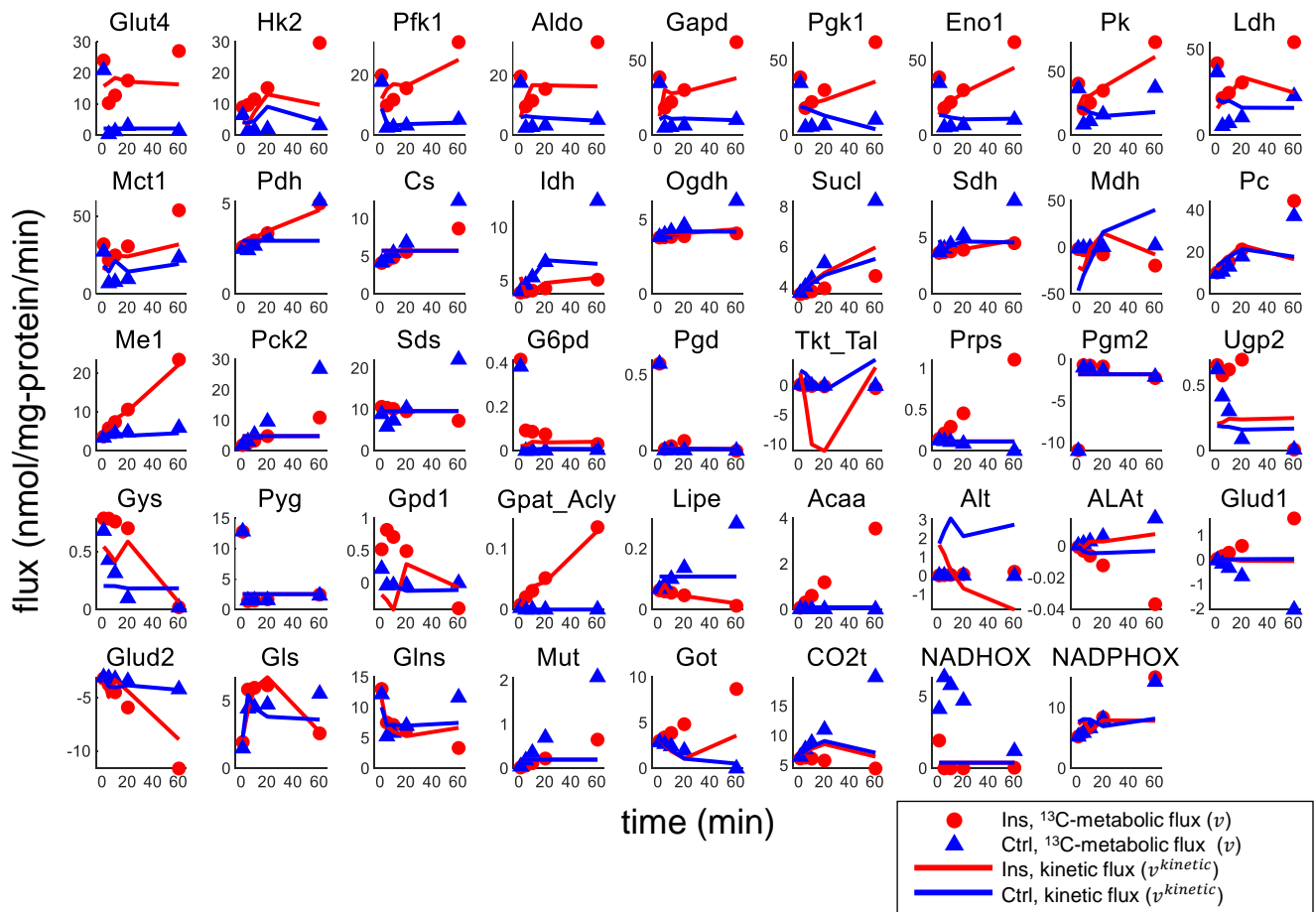


Figure S5. Time-averaged regulation coefficients and comparison of ^{13}C -metabolic fluxes with kinetic fluxes for all reactions. Related to Figure 6.

(A) Time-averaged regulation coefficients of enzyme phosphorylation (ρ_p), allosteric effectors (ρ_A), substrates and products (ρ_S), and unaccounted regulators (ρ_U). Error bars indicate the 90% confidence intervals. The confidence intervals were calculated from 200 sets of sampled parameters (see Transparent Methods). Note that the optimal estimates can be outside the confidence intervals due to sampling from a truncated multivariate normal distribution and the curse of dimensionality (Verleysen and François, 2005).

(B) Comparison of ^{13}C -metabolic fluxes (v), estimated by metabolic flux analysis under non-steady state conditions, with kinetic fluxes (v^{kinetic}) for all reactions. Abbreviations of reactions are defined in Table S1.

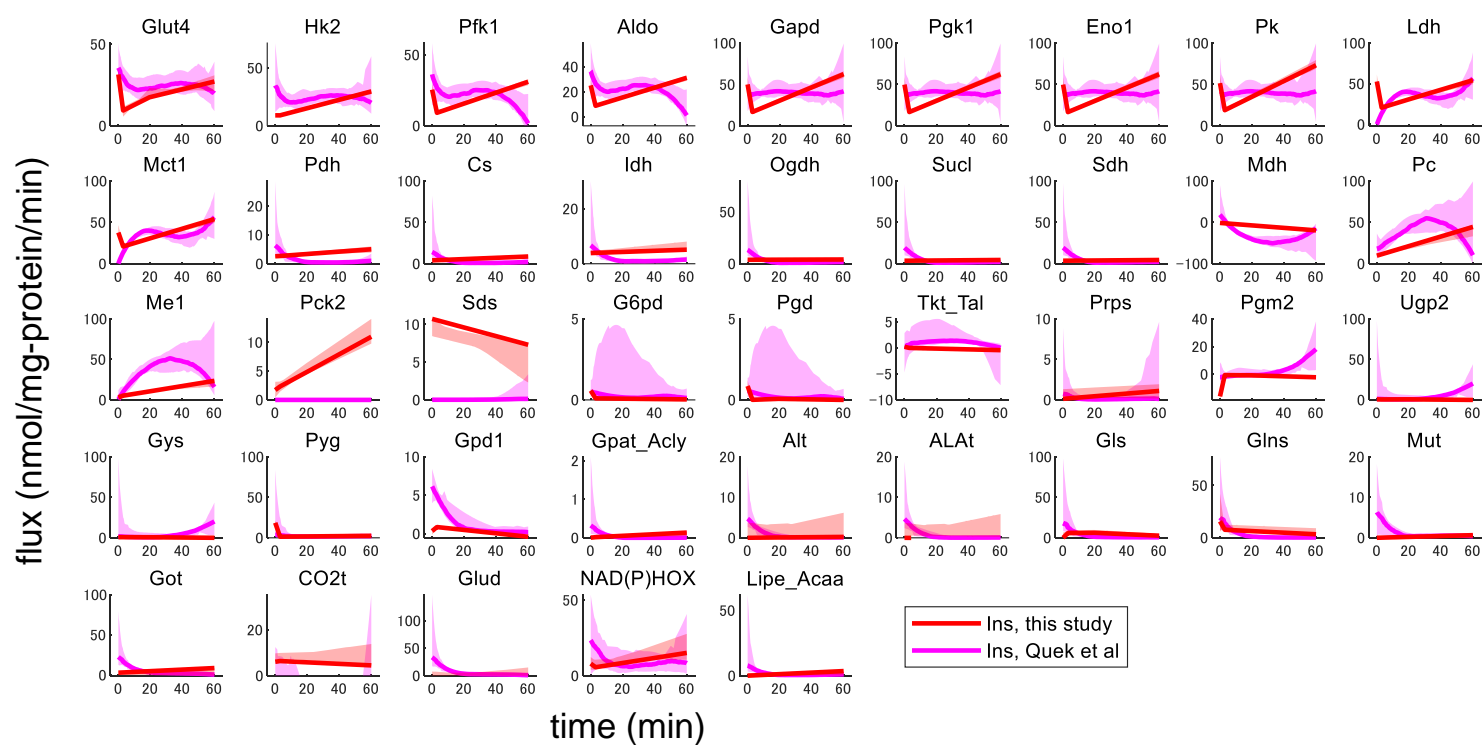
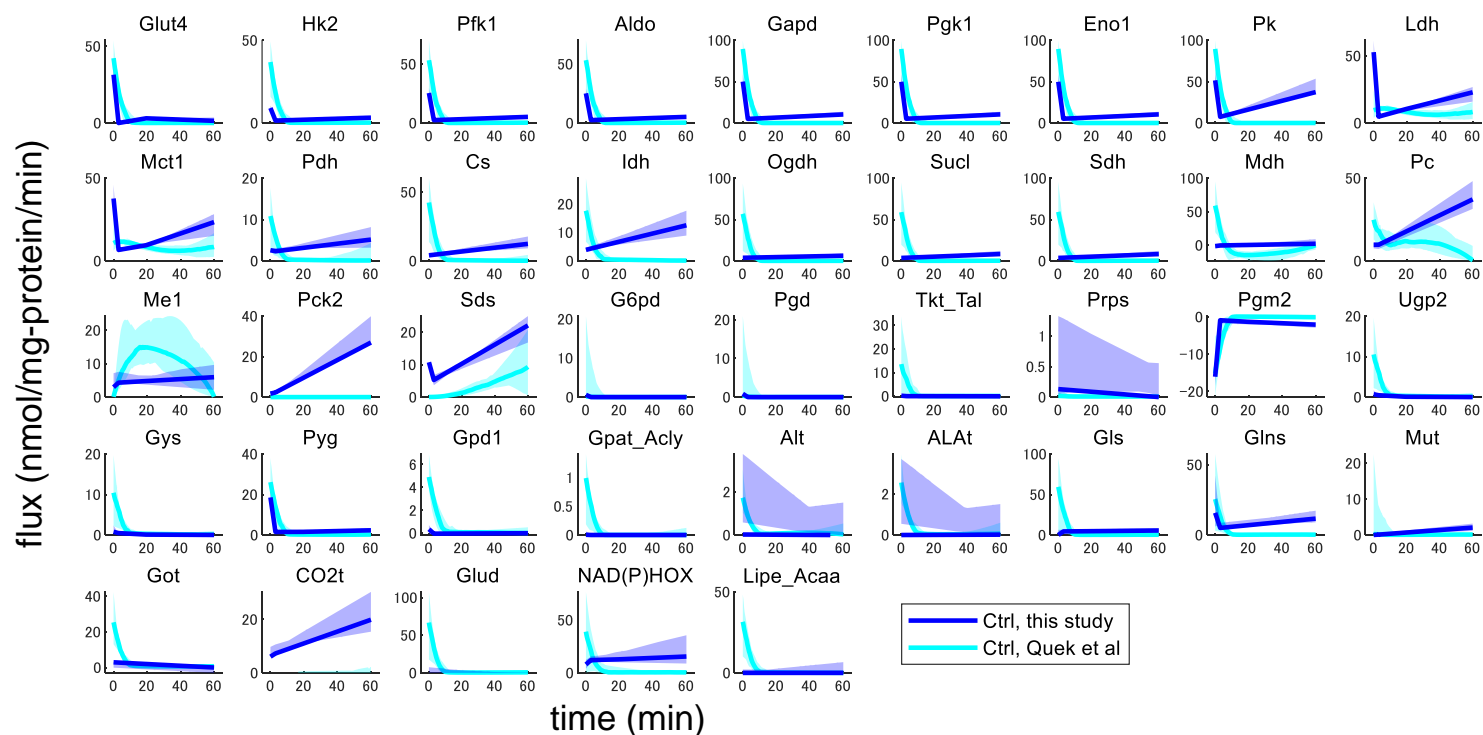
A**B**

Figure S6. Comparison of fluxes between this study and Quiek et al, 2020. Related to Figure 3.

(A-B) All of estimated flux changes in this study and Quiek et al, 2020 in the Ins (A) and Ctrl (B) conditions. In this study, the optimal estimates and the 90% confidence intervals are shown. In Quiek et al., the median values of fluxes among Monte-Carlo sampling and the 90% confidence intervals are shown. Abbreviations of reactions are defined in Data S1F.

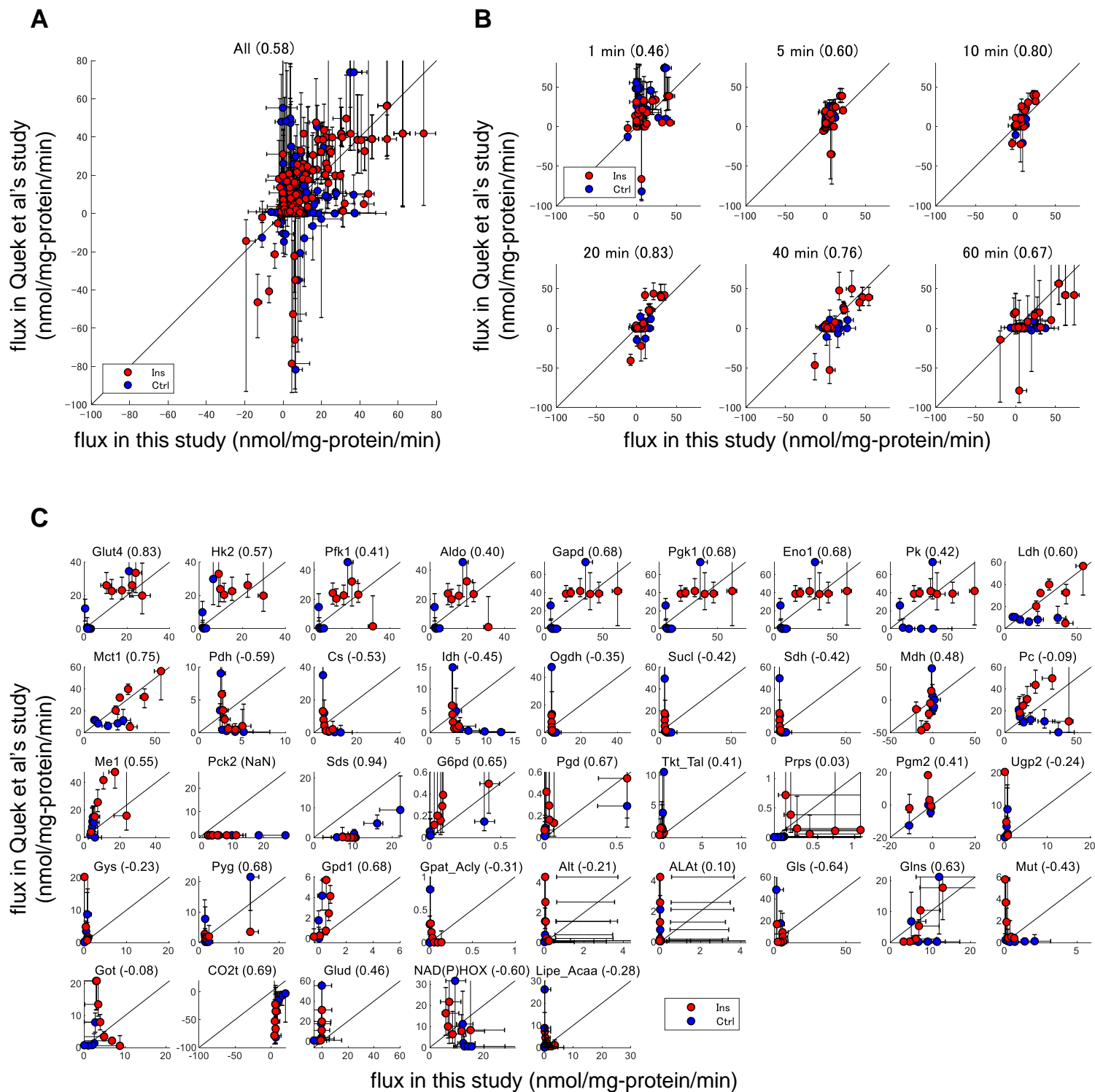


Figure S7. Scatter plots of estimated fluxes from this study and Quek et al, 2020. Related to Figure 3.

(A) Estimated fluxes through all reactions at all of 1, 5, 10, 20, 40, and 60 min. In this study, the optimal estimates and the 90% confidence intervals are shown. In Quek et al., 2020, the median values of fluxes among Monte-Carlo sampling and the 90% confidence intervals are shown. Pearson's correlation coefficients are shown in parentheses. Note that the optimal estimates in this study can be outside the confidence intervals due to sampling from a truncated multivariate normal distribution and the curse of dimensionality (Verleysen and François, 2005).

(B) Estimated fluxes through all reactions at each time point (1, 5, 10, 20, 40, and 60 min).

(C) Estimated fluxes through each reaction at all time points (1, 5, 10, 20, 40, and 60 min). Abbreviations of reactions are defined in Data S1F.

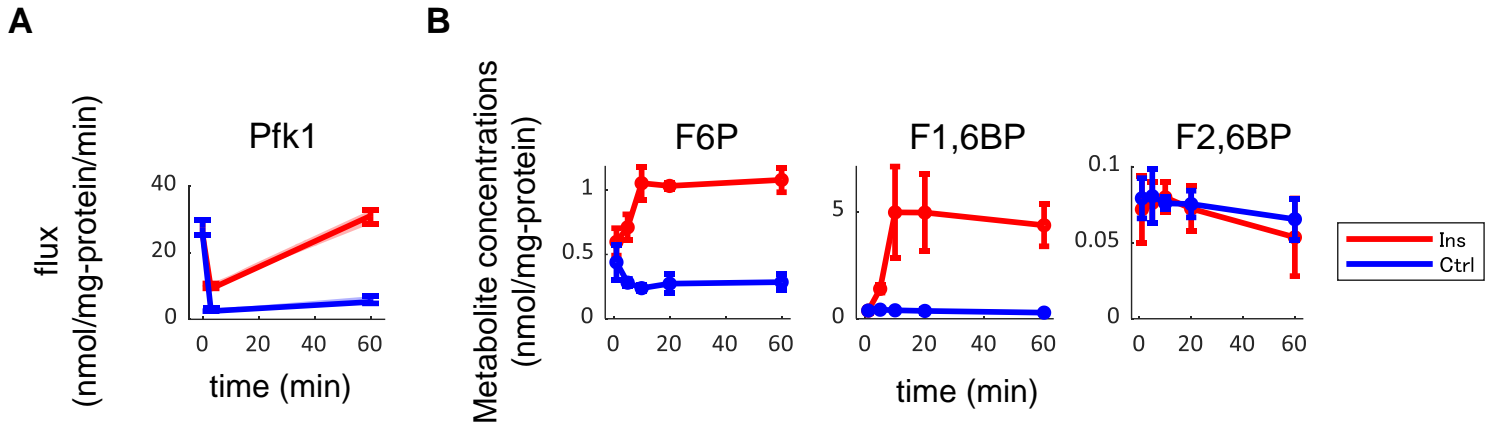


Figure S8. The estimated flux through Pfk1 and the measured amounts of F6P, F1,6BP and F2,6BP. Related to Figure 5.

(A) The estimated flux through Pfk1, same as in Figures 3B and S3.

(B) The measured amounts of F6P, F1,6BP and F2,6BP. The circles and the error bars indicate the mean and the standard deviations of the measurements from 3 separate experiments.

TRANSPARENT METHODS

¹³C-metabolic flux analysis under non-steady-state conditions

Metabolic network model

A metabolic network model was constructed for metabolic flux analysis under non-steady-state conditions (Figures 3A and Table S1). The model consists of 26 internal metabolites and 41 reactions (Table S1) and includes reactions of glycolysis, TCA cycle, PP pathway, anaplerotic reactions, glycogen synthesis and degradation, and TG synthesis and degradation. Although glucose production in adipocytes has not been reported (Cherrington, 1999), Pck2 was included in the model because Pck2 protein was expressed in adipocytes in our previous study (Humphrey et al., 2013).

Because G6P and F6P are adjacent and their isotopic ratios were similar, these metabolites were considered to be in rapid equilibrium and were summed as one metabolite, G6P_F6P for simplicity (Figure 3A, Table S1). Similar to G6P and F6P, malate and fumarate were summed as one metabolite, Mal_Fum, and citrate, aconitate, and isocitrate were summed as one metabolite as Cit_Acon_Icit. Also, 3-phosphogluconate and 2-phosphogluconate, and F1,6BP and F2,6BP were summed as one metabolite, 3PG_2PG and FBP, respectively, because these metabolites were not separated by capillary electrophoresis-mass spectrometry (CE-MS) under our experimental conditions (Krycer et al., 2017). It should be noted that F1,6BP and F2,6BP were separated by ion chromatography-mass spectrometry (IC-MS) as described later, but we used the summed FBP in the metabolic network for metabolic flux analysis to use intracellular metabolome data obtained under the same measurement condition.

In the PP pathway, ribose 5-phosphate, ribulose 5-phosphate, and xylulose 5-phosphate were summed as one metabolite as P5P because ribulose 5-phosphate and xylulose 5-phosphate were not measured in our previous study (Krycer et al., 2017). To simplify the network model, erythrose 4-phosphate (E4P) and sedoheptulose 7-phosphate (S7P) were omitted in the PP pathway, and reactions associated with E4P and S7P were merged as one reaction (Table S1).

In TG synthesis, one molecule of TG is synthesized from one molecule of glycerol 3-phosphate and three molecules of fatty acids through the Gpat reaction. Fatty acids are synthesized from citrate through a series of reactions, for which Acly reaction is the first and important step in fatty acid synthesis (Potapova et al., 2000). We assumed that adipocytes in this study have the same fatty acid composition of TG as adipocytes of rats in a previous study (Body, 1988), leading to average 17.1 carbon atoms in fatty acids in TG. Therefore, we defined TG synthesis reaction in the model as Gpat_Acly, where one molecule of TG is synthesised from one molecule of glycerol 3-

phosphate and 25.7 molecules of citrate. We did not include lipids other than TG in the model, because TG represents 90% of lipids in adipose tissue of animals (Body, 1988). Similar to TG synthesis, we described a reaction of TG degradation in which 25.8 molecules of acetyl-CoA are synthesized from one molecule of TG. ATP is not included in the model, because there are various reactions that consume ATP and including ATP would not affect overall fluxes in glucose metabolism. Compartmentation of reactions into cytoplasm and mitochondria was not considered and estimated fluxes using this model represents averaged fluxes, assuming a whole cell as a single compartment.

Flux change as a piecewise linear function of time

To model flux changes (Figures 2, 3 and Figures S1, S2, S3), we needed to describe flux changes as a function of time. Similar to previous studies (Abate et al., 2012; Leighty and Antoniewicz, 2011), flux changes were defined as a continuous piecewise linear function in the time domain with switch times (t_1, t_2, \dots, t_K) between t_0 (0 min) and t_{K+1} (60 min) (Figure S1B). Flux changes in a time interval between t_k and t_{k+1} were described by

$$\mathbf{v}(t) = \mathbf{v}_k + \frac{\mathbf{v}_{k+1} - \mathbf{v}_k}{t_{k+1} - t_k} (t - t_k), \quad t_k \leq t \leq t_{k+1}, \quad (1)$$

where \mathbf{v} is a vector of flux changes, and \mathbf{v}_k is a vector of fluxes at t_k . All functions for flux changes have the same switch times. Reversible reactions were modelled as separate forward and backward fluxes.

Equations for describing changes of metabolite concentrations over time under non-steady-state conditions

The mass balance equation of metabolites for flux estimation can be described by

$$\frac{d\mathbf{c}}{dt} = \mathbf{S}\mathbf{v}, \quad (2)$$

where \mathbf{c} is metabolite concentrations in the metabolic network, and \mathbf{S} is the stoichiometric matrix of the metabolic network. The integration of Equation (2) can be described by

$$\mathbf{c}(t) = \mathbf{c}_0 + \mathbf{S} \int_0^t \mathbf{v} dt. \quad (3)$$

Because \mathbf{v} is a vector of piecewise linear function of time, Equation (3) can be solved analytically. These equations were used to generate the graphs shown in Figure 2, Figure S2 and data in Table S2.

Equations for describing changes of mass isotopomer fractions over time under non-steady-state conditions

The elementary metabolite unit (EMU) framework (Antoniewicz et al., 2007; Young et al., 2008) was used to efficiently simulate mass isotopomer fractions (Figure 2, Figures S1 and S2). In EMU framework, a decomposition method is used to break isotopomers into EMUs to reduce computational burden. Each EMU includes a subset of metabolite atoms that are directly involved in precursor-product relationships. EMUs are organized into size blocks, for which size refers to the number of atoms included in the EMU. In EMU framework, mass isotopomer fractions of EMUs are sequentially simulated from smallest to largest size blocks.

Metabolic flux analyses using the EMU framework have been applied to metabolism under steady-state conditions (Young et al., 2008). Here, we developed an EMU framework that can be applied to metabolism under non-steady-state conditions. The EMU balance equations for n th size block under non-steady-state conditions can be expressed by

$$\frac{d \text{diag}(\mathbf{c}_n)\mathbf{x}_n}{dt} = \mathbf{A}_n\mathbf{x}_n + \mathbf{B}_n\mathbf{y}_n, \quad (4)$$

where \mathbf{x}_n is a vector of mass isotopomer fractions of EMUs. \mathbf{c}_n is a vector of concentrations corresponding to EMUs in \mathbf{x}_n , and $\text{diag}(\mathbf{c}_n)$ is a diagonal matrix whose elements are \mathbf{c}_n . \mathbf{y}_n is a vector of mass isotopomer fractions of EMUs that are previously simulated inputs to the n th size block. Each EMU that comprises the \mathbf{x}_n and \mathbf{y}_n vectors is defined by the metabolite name and the subset of atoms it includes. \mathbf{A}_n and \mathbf{B}_n are functions of flux (\mathbf{v}) and defined as follows:

$$\mathbf{A}_n(i, j) = \begin{cases} - \text{sum of fluxes consuming } i\text{th EMU in } \mathbf{x}_n, & i = j \\ \text{flux to } i\text{th EMU in } \mathbf{x} \text{ from } j\text{th EMU in } \mathbf{x}_n, & i \neq j \end{cases} \quad (5)$$

$$\mathbf{B}_n(i, j) = \text{flux to } i\text{th EMU in } \mathbf{x}_n \text{ from } j\text{th EMU in } \mathbf{y}_n. \quad (6)$$

Here, mass balance of metabolite concentrations corresponding to EMUs in \mathbf{x}_n can be described as follows:

$$\frac{d\mathbf{c}_n}{dt} = \mathbf{S}_n\mathbf{v}, \quad (7)$$

where \mathbf{S}_n is the stoichiometric matrix with each row representing the metabolite corresponding to EMUs in \mathbf{x}_n . By combining Equations (4) and (7), we can rewrite EMU balance equations:

$$\frac{d\mathbf{x}_n}{dt} = (\text{diag}(\mathbf{c}_n))^{-1}((\mathbf{A}_n - \text{diag}(\mathbf{S}_n\mathbf{v}))\mathbf{x}_n + \mathbf{B}_n\mathbf{y}_n). \quad (8)$$

We used Equation (8) to simulate mass isotopomer fractions of EMUs. Simulated mass isotopomer

fractions of a metabolite were obtained from the corresponding EMU with a size that is the same as the number of skeletal carbon atoms in the metabolite. Equation (8) was solved numerically using MATLAB function ode15s with absolute tolerance of 5×10^{-4} , relative tolerance of 5×10^{-4} , maximum order of formula of 3, and specified Jacobian sparsity pattern. Extracellular glucose was the only carbon source that uniformly labelled with ^{13}C and was assumed to have atomic purity of 99%.

Parameter estimation

Parameters θ including switch times (t_1, t_2, \dots, t_K), fluxes ($v_k, k \in \{0, 1, \dots, K + 1\}$), and initial metabolite concentrations (c_0) were estimated by minimizing the variance-weighted residual sum of squared errors (wRSS) between measured and simulated metabolite concentrations and mass isotopomer fractions according to the following equation (Figures 2 and 3, Figures S1 and S3):

$$\begin{aligned} \text{Min.}_{\theta} \quad & \text{wRSS} = (\mathbf{c}^{mes} - \mathbf{c})^T \Sigma_c^{-1} (\mathbf{c}^{mes} - \mathbf{c}) + (\mathbf{x}^{mes} - \mathbf{x})^T \Sigma_x^{-1} (\mathbf{x}^{mes} - \mathbf{x}), \\ \text{s. t.} \quad & \mathbf{c} \geq \mathbf{0}, \\ & \mathbf{c}_{0,\text{Ins}} = \mathbf{c}_{0,\text{Ctrl}}, \\ & \mathbf{v}_{0,\text{Ins}} = \mathbf{v}_{0,\text{Ctrl}}, \\ & \boldsymbol{\theta}^{\text{LB}} \leq \boldsymbol{\theta} \leq \boldsymbol{\theta}^{\text{UB}}, \\ & t_{k+1} > t_k + \epsilon, \quad k \in \{0, 1, \dots, K\}, \end{aligned} \quad (9)$$

where \mathbf{c}^{mes} and \mathbf{x}^{mes} are vectors of the measured metabolite concentrations and mass isotopomer fractions, respectively (Data S1A). Σ_c and Σ_x are diagonal matrices containing measurement variances of metabolite concentrations and mass isotopomer fractions, respectively. To avoid overfitting of metabolite concentrations and mass isotopomer fractions that were associated with an unusually small standard deviation (SD), the minimum SD of the measured metabolite concentration was set at 1% and the minimum SD of the measured mass isotopomer fraction was set at 0.01. $\mathbf{c}_{0,\text{Ins}}$ and $\mathbf{c}_{0,\text{Ctrl}}$ are the initial metabolite concentrations in the Ins and Ctrl conditions, respectively, and set to be the same. Similarly, $\mathbf{v}_{0,\text{Ins}}$ and $\mathbf{v}_{0,\text{Ctrl}}$ are the initial fluxes in the Ins and Ctrl conditions, respectively, and set to be the same. $\boldsymbol{\theta}^{\text{LB}}$ and $\boldsymbol{\theta}^{\text{UB}}$ are lower and upper bounds of $\boldsymbol{\theta}$, respectively (Data S1B). ϵ was set to 1.01 to avoid t_k and t_{k+1} getting too close.

We obtained measured concentrations of mass isotopomers that were corrected for natural abundances from our previous paper (Krycer et al., 2017), and identified measured concentrations of mass isotopomers with amounts that were measured 2 or more times in 3 separate experiments. We calculated measured concentration of metabolite m (c_m^{mes}) and measured fraction of mass isotopomer i of metabolite m ($x_{m,i}^{mes}$) as follows:

$$c_m^{mes} = \sum_i d_{m,i}^{mes}, \quad (10)$$

$$x_{m,i}^{mes} = \frac{d_{m,i}^{mes}}{\sum_i d_{m,i}^{mes}}, \quad (11)$$

where $d_{m,i}^{mes}$ is the measured concentration of mass isotopomer i of metabolite m . We also measured extracellular lactate and used this value for calculation of wRSS. Metabolites and mass isotopes used for calculating wRSS are shown in Data S1A. In total, we obtained 131 metabolite concentrations and 463 mass isotopomer fractions for the Ins condition, and 132 metabolite concentrations and 424 mass isotopomer fractions for the Ctrl condition.

The minimization problem of Equation (9) was numerically solved by a metaheuristic optimization of a covariance matrix adaptation evolution strategy (CMA-ES) with a negative update of the covariance matrix (Hansen and Kern, 2004) to approach the local minimum, followed by application of the interior point method to reach the local minimum using the MATLAB function `fmincon`. The initial population was sampled uniformly from the feasible region (Kaufman and Smith, 1998), and the mean and the covariance matrix were used as initial conditions for CMA-ES. The initial population size was set to 10^3 and the population size during the optimization was set to 50. The objective function of wRSS was evaluated at least 1.5×10^6 . Parameter estimation was performed for 30 times with each number of time intervals to obtain the best parameter sets with minimized wRSS. Parameters were optimised in a logarithmic scale for CMA-ES and in a linear scale for `fmincon`.

Introduction of quadratic programming during the metaheuristic optimization in the parameter estimation

Metabolic flux analysis under non-steady-state conditions requires more number of parameters and has a larger computation cost for optimization than metabolic flux analysis under steady-state conditions. We achieved faster optimization by introducing quadratic programming (QP) during the metaheuristic optimization (Figure S1E). Changes in metabolites concentrations can be described as piecewise quadratic functions as the integral of the piecewise linear functions of fluxes. Therefore, when independent parameters (θ^{MO}) including switch times are given, wRSS associated with only metabolite concentrations (wRSS^{QP}) can be minimized easily by QP where variables are the remaining parameters (θ^{QP}):

$$\begin{aligned} \text{Min.}_{\theta^{QP}} \quad & \text{wRSS}^{QP} = (\mathbf{c}^{mes} - \mathbf{c})^T \Sigma_c^{-1} (\mathbf{c}^{mes} - \mathbf{c}), \\ \text{s. t.} \quad & \mathbf{c} \geq \mathbf{0}, \\ & \mathbf{c} = \mathbf{A}^{QP}(\theta^{MO}) \cdot \theta^{QP} + \mathbf{b}^{QP}(\theta^{MO}), \\ & \theta^{QP, LB} \leq \theta^{QP} \leq \theta^{QP, UB}, \end{aligned} \quad (12)$$

where A^{QP} and b^{QP} are a matrix and a vector, respectively, with elements that are determined from θ^{MO} . We can identify which parameters are included in θ^{MO} from Equation (9) before metaheuristic optimization. When t_k are given, all constraints in Equation (9) become linear. A basis for the row space of the coefficient matrix in the linear equality constraints corresponds to a parameter included in θ^{QP} , whereas a non-basis corresponds to a parameter included in θ^{MO} . Note that the initial metabolite concentrations (c_0) were set to always be included in θ^{MO} . During the metaheuristic optimization using CMA-ES, we iteratively perturbed the independent parameters θ^{MO} , solved the QP problem in Equation (12) by the MATLAB function quadprog to obtain the other parameters θ^{QP} , and evaluated wRSS in Equation (9). By introducing QP problem, we obtained parameter sets with the smallest wRSS values within a small number of evaluations of wRSS (Figure S1F), possibly because of the reduction in search space from the entire solution space during metaheuristic optimization.

Estimation of confidence intervals of parameters

Confidence intervals of parameters were estimated from the Jacobian matrix of the minimized wRSS. Assuming that the estimates of the minimization problem [Eq. (9)] converges to a global minimum, the Hessian matrix H can be approximated from the Jacobian matrix J as follows:

$$H = J^T J. \quad (13)$$

The Jacobian matrix includes the partial derivatives of wRSS with respect to the model parameters. We calculated the inverse of the Hessian, which gives the local estimate for the parameter covariance matrix Σ_θ :

$$\Sigma_\theta = H^{-1}. \quad (14)$$

When we estimated fluxes using models for which the same number of time intervals was set among all reactions, confidence intervals of parameters were estimated based on linearized statistics as previously described (Antoniewicz et al., 2006). The diagonal elements of Σ_θ are the variances of the estimated parameters, from which the approximated 90% confidence intervals (CI) can be calculated as

$$CI_i = \theta_i^* \pm z \sqrt{\Sigma_{\theta(i,i)}}, \quad (15)$$

where θ^* is a vector of optimal estimates of the minimization problem [Eq. (9)], and z is the z-score for 90% confidence intervals (1.6449).

When we estimated fluxes using models under reaction-dependent number of time intervals, we sampled parameters for 200 times from a truncated multivariate normal distribution (Robert, 1995). The mean of the distribution was the optimal estimates of the minimization problem [Eq. (9)] and the

covariance matrix was Σ_{θ} . The constraints of the distribution were the same as the minimization problem [Eq. (9)]. The sampled parameters are shown in Data S1C. The 90% confidence intervals of the parameters were calculated from the distribution of the sampled parameters. This calculation of the 90% confidence intervals accounts for constraints, such as the positive metabolite concentration, and for calculation of the confidence intervals of regulation coefficients, which are estimated in subsequent analyses. Because the confidence intervals were calculated from sampled parameters from a truncated multivariate normal distribution, the optimal estimates of parameters can be outside the confidence intervals due to the curse of dimensionality (Verleysen and François, 2005).

We understand that measured data are often perturbed by a Monte Carlo procedure to estimate confidence intervals of parameters in metabolic flux analysis (Hörl et al., 2013; Quek et al., 2020). However, applying a Monte Carlo procedure to our metabolic flux analysis would not be practical, because our metabolic flux analysis under non-steady-state conditions requires a large computational cost due to many number of parameters in optimization and many number of ODEs to be solved numerically. In our metabolic flux analysis, computational time of parameter estimation for one condition (e.g. experimental conditions and number of time intervals) was over 1.5 months on an AMD EPYC7501 processor on a Linux machine. Instead, we estimated confidence intervals of parameters from the inverse of the Hessian matrix of the minimized the variance-weighted residual sum of squared errors. The method we used is a general method to calculate confidence intervals in an approximate manner, and the computational cost is smaller than Monte Carlo procedures. We adopted appropriate methods of optimization and estimation of confidence intervals to match the complexity of our metabolic flux analysis under non-steady-state conditions.

Determination of reaction-dependent number of time intervals

Number of time intervals (or number of switch times) of fluxes should be selected for flux analysis under non-steady-state conditions (Figure 3, Figure S1). The number of time intervals cannot be selected by solving the optimization problem of Equation (9). More time intervals can potentially provide more accurate estimation of flux changes, which means smaller differences between measurements and estimates; however, more time intervals require more parameter numbers and less precise estimation, which means larger sensitivity to measurement errors.

Here, we propose a method to determine reaction-dependent number of time intervals, in which the number of time interval in each reaction can be independently determined (Figure S1C, D). First, we developed models in which the same number of time intervals was set among all

reactions, and estimated fluxes and their approximated confidence intervals as defined in Equation (15). The number of time intervals was either of one, two, or three. Next, we compared confidence intervals of each flux between models under one and two time interval(s). Because a higher number of time intervals may decrease estimation precision (as seen for Ogdh in Figure S1C), we selected the time interval of one for the reaction if confidence intervals for all time points were the same in models with one or two time intervals.

If confidence intervals for any time points were not the same for models with one or two time intervals, we tentatively selected two time intervals for the reaction because the lower number of time intervals may provide a less accurate estimation of flux changes (as seen for Pfk1 in Figure S1C). Reactions for which two time intervals are tentatively selected, we compared the confidence intervals for models with two or three time intervals and selected the number of time intervals using the same criterion that were used to select between one and two time intervals.

Because the confidence intervals used to determine the number of time intervals depend on z-score (or percentage for the confidence intervals), we generated 10 models using different z-scores for the calculation of the confidence intervals. Smaller z-scores lead to narrower confidence intervals and result in models with a larger number of parameters. We performed metabolic flux analysis using each of the generated models and selected the model with the smallest AIC as the final model with a reaction-dependent number of time intervals. The AIC value of the final model is smaller than the any of the models with the same number of time intervals among all reactions (Figure S1D), indicating that the model with a reaction-dependent number of time intervals is statistically more appropriate than models with the same number of time intervals among all reactions. This method reduced computation cost compared to methods for selecting time intervals from all possible combinations of the number of time intervals.

Estimation of glucose uptake, ¹⁴C-glycogen accumulation, ¹⁴C-fatty acid accumulation in TG and ¹⁴C- CO₂ secretion

To validate the estimated flux from other experiments using natural glucose or ¹⁴C-glucose as a tracer (Figure 4), we estimated glucose uptake, ¹⁴C-glycogen accumulation, ¹⁴C-fatty acid accumulation in TG, and ¹⁴C-CO₂ secretion using the model and the estimated fluxes. These estimates were calculated using the estimated flux v through reaction j from substrate k to product l and the estimated fractions of $M+i$ mass isotopomer of a substrate k :

$$-n_k \cdot S_{k,j} \cdot r_{j,k,l} \int_0^{60} v_j(t) \frac{\sum_{i=0}^{n_k} i \cdot x_{k,i}(t)}{n_k} dt, \quad (16)$$

where n_k is the number of skeletal carbon atoms in substrate k . $S_{k,j}$ is the stoichiometric coefficient of substrate k in reaction j and is a negative value. $r_{j,k,l}$ is the ratio of carbon atoms in substrate k that is transferred to product l through reaction j .

For glucose uptake, the substrate is extracellular glucose, the product is intracellular glucose, and the reaction is Glut4. For ^{14}C -glycogen accumulation, the substrate is UDP-glucose, the product is glycogen, and the reaction is Gys. For ^{14}C -fatty acid accumulation in TG, the substrate is Cit_Acon_IsoCit, the product is TG, and the reaction is Gpat_Acly. For ^{14}C - CO_2 secretion, the substrate is the intracellular CO_2 , the product is the extracellular CO_2 , and the reaction is the CO_2 transporter (CO2t). $r_{j,k,l}$ is 0.33 for ^{14}C -fatty acid accumulation in TG and 1 for the others.

Identification of key regulatory mechanisms in the glucose metabolism in insulin-stimulated adipocytes

An overview of the description of flux based on reaction kinetics is shown in Figure 5A. In addition to substrates and products, we included enzyme phosphorylation and allosteric effectors that can potentially regulate fluxes in addition to substrates and products. We obtained enzyme phosphorylation results that were classified as Class I (a phosphorylation site localization probability score derived from MaxQuant (Cox and Mann, 2008) > 0.75) in phosphoproteomic data (Humphrey et al., 2013). We obtained information of reported allosteric effectors for *Mus musculus*, *Rattus norvegicus*, and *Homo sapiens* in the BRENDA database using the Simple Object Access Protocol (SOAP) with Perl (Placzek et al., 2017). We obtained the amounts of phosphorylation and allosteric effectors from phosphoproteomic and metabolomics data in previous studies (Humphrey et al., 2013; Krycer et al., 2017), respectively, and identified enzyme phosphorylation and allosteric effectors with amounts that were measured 2 or more times in 3 separate experiments. In total, 82 phosphorylation sites (80 unique sites on 25 enzymes) and 170 allosteric effectors together with substrates and products were obtained as candidates of regulatory molecule (Table S3).

Reaction kinetic equation

We developed models for each reaction in which flux is described as a modular rate law (Liebermeister et al., 2010) (Figure 5A). We used common modular with complete activation or inhibition and we set all relevant regulation numbers to a value of one, assuming no cooperativity. In the model selection, we develop a model containing k_1 and only a function of substrate and products, and we also develop models containing one or more functions of enzyme phosphorylation

and allosteric effectors, as well as k_1 and the function of substrates and products. For each reaction, flux $v^{kinetic}$ is defined as a product of kinetic constant k_1 and functions of amounts of substrates and products, enzyme phosphorylation, and allosteric effectors:

$$v^{kinetic} = k_1 \cdot f_S \cdot \prod_{i \in U_P} f_{P,i} \cdot \prod_{j \in U_A} f_{A,j}, \quad (17)$$

$$f_S = \frac{\prod(c_S/K_S) - k_2 \prod(c_P/K_P)}{\prod(1 + c_S/K_S) + \prod(1 + c_P/K_P) - 1}, \quad (18)$$

$$f_{P,i} = \begin{cases} \frac{P_i}{K_{PE,i} + P_i}, & \text{if } i\text{-th enzyme phosphorylation is an activator,} \\ \frac{K_{PE,i}}{K_{PE,i} + P_i}, & \text{if } i\text{-th enzyme phosphorylation is an inhibitor,} \end{cases} \quad (19)$$

$$f_{A,j} = \begin{cases} \frac{C_{A,j}}{K_{A,j} + C_{A,j}}, & \text{if } j\text{-th allosteric effector is an activator,} \\ \frac{K_{A,j}}{K_{A,j} + C_{A,j}}, & \text{if } j\text{-th allosteric effector is an inhibitor,} \end{cases} \quad (20)$$

where f_S is a function of substrate and products (generalized Michaelis-Menten kinetics). U_P and U_A are the sets of candidate enzyme phosphorylation and allosteric effectors, respectively, that affect the flux as activators or inhibitors and the union of U_P and U_A is defined as U . $f_{P,i}$ is a function of i -th enzyme phosphorylation. Enzyme phosphorylation was considered for both cases of either an activator or an inhibitor. $f_{A,j}$ is a function of j -th allosteric effector. Allosteric effectors were considered as activators or inhibitors according to information in BREDNA database (Placzek et al., 2017). c_S , c_P , and c_A are amounts of the substrate, product, and allosteric effector, respectively, and their amounts were obtained from metabolomics data (Krycer et al., 2017) otherwise from estimated amounts of metabolites in our metabolic flux analysis. Note that summed metabolites in the metabolic flux analysis were separated in this analysis (for example, G6P_F6P was separated into G6P and F6P) and separated amounts were used for c_S and c_A . F1,6BP and F2,6P were summed as FBP in the metabolic flux analysis. Here, we measured F1,6BP and F2,6BP separately by IC-MS and the amount of each of F1,6BP and F2,6BP were used for c_S and c_A . 3PG and 2PG can not be separated by our measurement condition and only summed amounts ($c_{3PG,2PG}$) were available. We assumed 3PG and 2PG were close to equilibrium and we calculated separate amounts of 3PG (c_{3PG}) and 2PG (c_{2PG}) from $c_{3PG} + c_{2PG} = c_{3PG,2PG}$ and $c_{2PG}/c_{3PG} = K_{eq}$, where K_{eq} is 5.38 at pH = 7.2 and ionic strength = 0.15 M (Haraldsdóttir et al., 2012) according to eEquilibrator (Noor et al., 2013). P_i is an amount of i -th phosphorylation at a site of an enzyme. Amounts of

enzyme phosphorylation in the Ins condition were obtained from phosphoproteomic data in adipocytes in our previous study (Humphrey et al., 2013), while amounts of enzyme phosphorylation in the Ctrl conditions were set equal to the amount of enzyme phosphorylation at 0 min. k_1 and k_2 are kinetic constants. K_S , K_P , K_{PE} and K_A are affinity constants for the substrate, product, enzyme phosphorylation and allosteric effectors, respectively. We assumed that enzyme amounts remain constant and can be included in k_1 , because our carbon labelling experiments (60 min) was much shorter than 31 hours of median half-life of proteins (Sandoval et al., 2013). c_S , c_P , c_A and P were normalized by the L^2 norm before the following parameter estimation.

Parameter estimation

Kinetic parameters $\theta^{kinetic}$, including $k_1, k_2, K_S, K_P, K_{PE}$ and K_A , were estimated for each reaction using each model by minimizing the residual sum of squared errors (RSS) between fluxes defined by the modular rate law and the fluxes estimated by metabolic flux analysis in a logarithmic scale (Figure 5A):

$$\underset{\theta^{kinetic}}{\text{Min.}} \text{ RSS} = (\log \mathbf{v}' - \log \mathbf{v}^{kinetic}(\theta^{kinetic}))^T (\log \mathbf{v}' - \log \mathbf{v}^{kinetic}(\theta^{kinetic})), \quad (21)$$

where \mathbf{v}' is the fluxes estimated by metabolic flux analysis and is normalized by the L^2 norm. RSS was calculated from data at 1, 5, 10, 20, and 60 min, which is the shared time points between metabolomic and phosphoproteomic data in the Ins and Ctrl conditions. The minimization problem of Equation (21) was numerically solved by CMA-ES with a negative update of the covariance matrix, followed by interior point method using MATLAB function `fmincon` as applied to our metabolic flux analysis. The population size and the maximum number of RSS evaluations in CMA-ES was set to 30 and 10^4 , respectively. Parameter estimation was performed five times to obtain the best parameter sets with minimized RSS for each reaction using each model.

Model selection

Because not all enzyme phosphorylation and allosteric effectors effectively change the enzymatic activity and regulate fluxes, we identified enzyme phosphorylation and allosteric effectors that, together with substrates and products, effectively regulated fluxes using model selection (Figure 5A). We used AIC as the selection criterion for the model selection:

$$\text{AIC} = N \log \frac{\text{RSS}}{N} + 2p, \quad (22)$$

where N is the number of residuals and p is the number of kinetic parameters in the model. We performed model selection to determine $U (=U_P \cup U_A)$ using a stepwise selection method based on

AIC according to the following procedure (Yamashita et al., 2007):

(i) Set the subset U as an empty set, estimate the set of parameters that minimizes RSS, and calculate AIC. Here, U is temporarily set as the subset that minimizes AIC. Hereafter, we denoted the complementary set of U as U^c , and the size of the subset U as $\#U$.

(ii) For each candidate regulatory molecule i in U^c , add the i to U (denoted as U_i), estimate the set of parameters that minimizes RSS, and calculate AIC [denoted as $AIC(U_i)$].

(iii) Select $U^* = \underset{U_i}{\operatorname{argmin}} AIC(U_i)$ from $\#U^c$ candidates defined in step (ii). If $AIC(U) > AIC(U^*)$,

update U with U^* . If $AIC(U) \leq AIC(U^*)$, go to step (vi).

(iv) For each regulatory molecule j in U , remove the j from U (denoted as U_j), estimate the set of parameters that minimizes RSS, and calculate AIC [denoted as $AIC(U_j)$].

(v) Select $U^* = \underset{U_j}{\operatorname{argmin}} AIC(U_j)$ from $\#U$ candidates defined in step (iv). If $AIC(U) > AIC(U^*)$,

update U with U^* , and go to step (iv). If $AIC(U) \leq AIC(U_j)$, go to step (ii).

(vi) stop stepwise method.

We qualitatively identified the regulatory molecules in the final U with the smallest AIC. This model selection was performed for each reaction independently. The estimated parameters are shown in Data S1D.

Calculation of regulation coefficients

To quantify contributions of regulatory events by substrates, products, and the selected enzyme phosphorylation, or allosteric effectors, as well as unaccounted regulators to the estimated flux differences between the Ins and Ctrl conditions, we calculated a regulation coefficient ρ (Figure 5A). Similar approaches have been reported in previous studies (Gerosa et al., 2015; Hackett et al., 2016; ter Kuile and Westerhoff, 2001). Using the estimated kinetic parameters, the normalized flux estimated by metabolic flux analysis can be described for each point in each reaction as follows:

$$v' = k_1 \cdot f_S \cdot \prod_i f_{P,i} \cdot \prod_j f_{A,j} \cdot f_U, \quad (23)$$

where f_U is $v'/v^{kinetic}$, calculated from a residual in Equation (21). Variance of the fluxes in a logarithmic scale between the Ins and Ctrl conditions can be written as follows:

$$\sigma_{\log v}^2 = \left(\frac{\partial \log v'}{\partial \log \mathbf{f}} \right)^T \Sigma_{\log f} \left(\frac{\partial \log v'}{\partial \log \mathbf{f}} \right), \quad (24)$$

where $\sigma_{\log v}^2$ is the variance of the fluxes at a logarithmic scale. \mathbf{f} is a vector of f_S , f_P , f_A , and f_U , and $\Sigma_{\log f}$ is the covariance matrix of $\log \mathbf{f}$ and the diagonal elements of $\Sigma_{\log f}$ is the variance of $\log \mathbf{f}$ ($\sigma_{\log f}^2$) between the Ins and Ctrl conditions. According to Equation (23), the partial derivative of $\log v'$ with respect to each $\log f$ equals to one. We made the simplifying assumption that covariance between $\log \mathbf{f}$ is negligible and therefore $\Sigma_{\log f}$ is diagonal:

$$\sigma_{\log v}^2 \approx \sum \sigma_{\log f}^2. \quad (25)$$

We defined a regulation coefficient ρ as the contribution of each of identified enzyme phosphorylation and allosteric effectors, substrates and products, and unaccounted regulators to the flux difference between the Ins and Ctrl conditions, which is calculated by normalizing $\sigma_{\log f}^2$ at each time in Equation (25):

$$\rho = \frac{\sigma_{\log f}^2}{\sum \sigma_{\log f}^2}. \quad (26)$$

A regulation coefficient can take values from zero to one. Here, the variance between two conditions of Ins and Ctrl ($\sigma_{\log f}^2$) can be written by the difference between the two conditions ($\Delta \log f$):

$$\sigma_{\log f}^2 = \left(\frac{\Delta \log f}{2} \right)^2. \quad (27)$$

By combining Equations (26) and (27), we can rewrite regulation coefficients:

$$\left\{ \begin{array}{l} \rho_{P,i} = \frac{(\Delta \log f_{P,i})^2}{\sum (\Delta \log f)^2}, \\ \rho_{A,j} = \frac{(\Delta \log f_{A,j})^2}{\sum (\Delta \log f)^2}, \\ \rho_S = \frac{(\Delta \log f_S)^2}{\sum (\Delta \log f)^2}, \\ \rho_U = \frac{(\Delta \log f_U)^2}{\sum (\Delta \log f)^2}, \end{array} \right. \quad (28)$$

where $\rho_{P,i}$ stands for contribution of phosphorylation at site i to the flux difference between the Ins and Ctrl conditions and summation of $\rho_{P,i}$ for each reaction at each time point is denoted as ρ_P . $\rho_{A,j}$ stands for contribution of allosteric effector j , and summation of $\rho_{A,j}$ is denoted as ρ_A . ρ_S , and ρ_U stand for contributions of substrates and products, and unaccounted regulators, respectively. We calculated regulation coefficients at 1, 5, 10, 20, and 60 min, which are the same as the time points used for the kinetic parameter estimation. We linearly interpolated the regulation coefficients between the time points, and calculated a time-averaged regulation coefficient by the following:

$$\text{time-averaged } \rho = \frac{\int_1^{60} \rho(t) dt}{\int_1^{60} dt}. \quad (29)$$

Estimation of confidence intervals of regulation coefficients

To estimate confidence intervals of regulation coefficients (Figure 6A, Figures S4 and S5), we used the sampled parameters for the estimation of confidence intervals in the metabolic flux analysis (Data S1C). For each reaction in each sampling, we performed kinetic modelling with model selection and calculated the regulation coefficients. Amounts of enzyme phosphorylation were sampled from a normal distribution with a mean and a variance from the phosphoproteomic data (Humphrey et al., 2013). Amounts of allosteric effectors, substrates, and products were obtained from a normal distribution with a mean and a variance from the metabolomics data (Krycer et al., 2017); otherwise the amounts were from the sampled parameters. We identified the regulatory molecules in the model finally selected (Table S3) and calculated regulation coefficients using each set of the sampled or obtained amounts of enzyme phosphorylation, allosteric effectors, substrates, and products, as well as the fluxes (Table S4). The 90% confidence intervals of regulation coefficients including ρ_P , ρ_A , ρ_S , and ρ_U were calculated from the distribution of the regulation coefficients.

Determination of key regulatory molecules

Reactions with the 90% confidence interval of time-averaged ρ above zero were further analysed to determine key regulatory molecules in glucose metabolism in insulin-stimulated adipocytes. We focused on how many time each regulatory molecule was selected among 200 model selections using sampled parameters, and regarded the most selected regulatory molecules for each reaction as the key regulatory molecule that represent flux through the reaction.

Michaelis-Menten constants from the BRENDA database

Michaelis-Menten constants were obtained from the BRENDA database (Placzek et al., 2017) based on EC numbers. The Perl implementation of the Simple Object Access Protocol (SOAP::Lite) was employed to extract the K_M values in *Mus musculus*, *Rattus norvegicus*, *Homo sapiens*, *Bos taurus*, *Sus scrofa*, *Canis lupus familiaris*, and *Mammalia*. The exported data were further processed to remove entries for mutant enzymes. K_M values with three or more reports for a substrate or a product of a reaction were selected (Data S1E), and the geometric mean and the geometric standard deviations were calculated and compared with estimated values (Figure S4B).

Experimental methods

Metabolomic and phosphoproteomic data in insulin-stimulated adipocytes

For metabolic flux analysis and key regulatory mechanisms, we used metabolomic and phosphoproteomic data from insulin-stimulated adipocytes in our previous studies (Humphrey et al., 2013; Krycer et al., 2017; Quek et al., 2020) and the experimental procedures of the previous studies are briefly described below. For metabolomic measurements (Krycer et al., 2017; Quek et al., 2020), differentiated 3T3-L1 adipocytes were labelled with [U-¹³C] glucose (25 mM, 99 atom % ¹³C) and treated with 100 nM insulin or vehicle (PBS) for 1, 5, 10, 20, 40, or 60 min. Labelling with ¹³C and the treatment with 100 nM insulin or vehicle were started at the same time. Cell lysates and the culture media were analysed by CE-MS and liquid chromatography-mass spectrometry (LC-MS), respectively. For phosphoproteomic measurements (Humphrey et al., 2013), 3T3-L1 fibroblasts were triple SILAC labelled, differentiated into adipocytes, and treated with 100 nM insulin or vehicle (PBS) for 15 s, 30 s, 1 min, 2 min, 5 min, 10 min, 20 min, or 60 min. Proteins were acetone precipitated, resuspended in urea, reduced, alkylated, and digested with endoproteinase Lys-C followed by trypsin. Peptides were desalted and fractionated by strong cation exchange (SCX) and TiO₂ for phosphopeptide analysis. Eluted peptides were analysed by quantitative mass spectrometry.

Measurement of F1,6BP and F2,6BP by IC-MS

We measured F1,6BP and F2,6BP in the same samples of our previous study (Krycer et al., 2017). Capillary IC-MS analysis was performed using a Dionex ICS-5000+ system equipped with a Q Exactive Orbitrap MS system (Thermo Fisher Scientific, San Jose, CA) (Hirayama et al., 2020). The IC system consisted of a capillary pump, an eluent generator with a capillary KOH cartridge, an anion capillary electrolytic suppressor (ACES 300), and a conductivity detector. Ultrapure water was used as both the eluent and regenerant in the suppressor. Sample injection was performed with a Dionex WPS-3000TBPL autosampler. An Agilent 1100 series capillary HPLC pump (Agilent Technologies Deutschland GmbH, Waldbronn, Germany) was used to deliver the make-up solution.

Anionic metabolites were separated on a Dionex IonPac AS11-HC-4 µm column (250 × 0.4 mm, 4 µm; Thermo Fisher Scientific) that was maintained at 35°C. The flow rate was 20 µL/min and the injection volume was 0.4 µL. The following KOH concentration gradient was used: 1 mmol/L from 0 min to 2 min, 20 mmol/L at 16 min, 100 mmol/L at 35 min, held at 100 mmol/L until 40 min, and then

decreased to the initial concentration within 0.1 min and held at this concentration for 5 min. The total analysis time was 45.1 min. Isopropanol containing 0.1% acetic acid was delivered as the make-up solution at 5 $\mu\text{L}/\text{min}$.

The standard ESI sprayer (product number OPTON–20011, Thermo Fisher Scientific), without any alterations, was used in this study. The standard ESI sprayer contains two coaxial tubes. A fused-silica capillary (0.10 mm I.D., 0.19 mm O.D.), through which the eluent flowed, was inserted in a stainless-steel tube with a slightly larger diameter (first tube). A make-up solution was supplied through this tube and mixed with the eluent at the outlet of the sprayer. In addition, the sheath gas which assists with stable spray formation was supplied from the second coaxial tube.

The Q Exactive mass spectrometer was operated in ESI negative ion mode and the spray voltage was set at 4.0 kV. The capillary temperature was 300 °C, the sheath gas flow rate was 20 (arbitrary units), the auxiliary gas flow rate was 10 (arbitrary units), the sweep gas flow rate was 0 (arbitrary units), and the S-lens was 50 (arbitrary units). Full scan mode was used and the parameters were as follows: resolution, 70,000; auto gain control target, 1×10^6 ; maximum ion injection time, 100 ms; and scan range, 70–1000 m/z. The instrument was calibrated at the beginning of each sequence using the calibration solution provided by the instrument manufacturer.

Quantification and statistical analysis

All statistical details including statistical tests used, exact value of n, what n represents, definition of centre, and dispersion measures are described in the figure legends.

SUPPLEMENTAL REFERENCES

- Antoniewicz, M.R., Kelleher, J.K., and Stephanopoulos, G. (2006). Determination of confidence intervals of metabolic fluxes estimated from stable isotope measurements. *Metab. Eng.* 8, 324–337.
- Antoniewicz, M.R., Kelleher, J.K., and Stephanopoulos, G. (2007). Elementary metabolite units (EMU): A novel framework for modeling isotopic distributions. *Metab. Eng.* 9, 68–86.
- Body, D.R. (1988). The lipid composition of adipose tissue. *Prog. Lipid Res.* 27, 39–60.
- Cherrington, A.D. (1999). Banting Lecture 1997. Control of glucose uptake and release by the liver in vivo. *Diabetes* 48, 1198–1214.
- Cox, J., and Mann, M. (2008). MaxQuant enables high peptide identification rates, individualized p.p.b.-range mass accuracies and proteome-wide protein quantification. *Nat. Biotechnol.* 26, 1367–1372.
- Hansen, N., and Kern, S. (2004). Evaluating the CMA Evolution Strategy on Multimodal Test Functions. (Springer, Berlin, Heidelberg), pp. 282–291.
- Haraldsdóttir, H.S., Thiele, I., and Fleming, R.M.T. (2012). Quantitative assignment of reaction directionality in a multicompartmental human metabolic reconstruction. *Biophys. J.* 102, 1703–1711.
- Hörl, M., Schnidder, J., Sauer, U., and Zamboni, N. (2013). Non-stationary ¹³C-metabolic flux ratio analysis. *Biotechnol. Bioeng.* 110, 3164–3176.
- Kaufman, D.E., and Smith, R.L. (1998). Direction Choice for Accelerated Convergence in Hit-and-Run Sampling. *Oper. Res.* 46, 84–95.
- ter Kuile, B.H., and Westerhoff, H. V (2001). Transcriptome meets metabolome: hierarchical and metabolic regulation of the glycolytic pathway. *FEBS Lett.* 500, 169–171.
- Leighty, R.W., and Antoniewicz, M.R. (2011). Dynamic metabolic flux analysis (DMFA): a framework for determining fluxes at metabolic non-steady state. *Metab. Eng.* 13, 745–755.
- Noor, E., Haraldsdóttir, H.S., Milo, R., and Fleming, R.M.T. (2013). Consistent Estimation of Gibbs Energy Using Component Contributions. *PLoS Comput. Biol.* 9.
- Robert, C.P. (1995). Simulation of truncated normal variables. *Stat. Comput.* 5, 121–125.
- Sandoval, P.C., Slentz, D.H., Pisitkun, T., Saeed, F., Hoffert, J.D., and Knepper, M.A. (2013). Proteome-wide measurement of protein half-lives and translation rates in vasopressin-sensitive collecting duct cells. *J. Am. Soc. Nephrol.* 24, 1793–1805.
- Young, J.D., Walther, J.L., Antoniewicz, M.R., Yoo, H., and Stephanopoulos, G. (2008). An elementary metabolite unit (EMU) based method of isotopically nonstationary flux analysis. *Biotechnol. Bioeng.* 99, 686–699.